Isoscalar $\pi\pi$ Scattering and the σ Meson Resonance from QCD

Raul A. Briceño,[1,*] Jozef J. Dudek,[1,2,†] Robert G. Edwards,[1,‡] and David J. Wilson[3,§]

(for the Hadron Spectrum Collaboration)

[1]*Thomas Jefferson National Accelerator Facility, 12000 Jefferson Avenue, Newport News, Virginia 23606, USA*
[2]*Department of Physics, College of William and Mary, Williamsburg, Virginia 23187-8795, USA*
[3]*Department of Applied Mathematics and Theoretical Physics, Centre for Mathematical Sciences,*
University of Cambridge, Wilberforce Road, Cambridge CB3 0WA, United Kingdom

We present for the first time a determination of the energy dependence of the isoscalar $\pi\pi$ elastic scattering phase shift within a first-principles numerical lattice approach to QCD. Hadronic correlation functions are computed including all required quark propagation diagrams, and from these the discrete spectrum of states in the finite volume defined by the lattice boundary is extracted. From the volume dependence of the spectrum, we obtain the S-wave phase shift up to the $K\bar{K}$ threshold. Calculations are performed at two values of the u, d quark mass corresponding to $m_\pi = 236, 391$ MeV, and the resulting amplitudes are described in terms of a σ meson which evolves from a bound state below the $\pi\pi$ threshold at the heavier quark mass to a broad resonance at the lighter quark mass.

Introduction.—Meson-meson scattering has long served as a tool to investigate the fundamental theory of strong interactions, quantum chromodynamics (QCD). The isoscalar channel, where all flavor quantum numbers are equal to 0, is dominated at low energies by $\pi\pi$ scattering, but despite experimental data on elastic $\pi\pi$ scattering being in place for many decades [1], the existence of the lowest-lying resonance with spin zero, the $f_0(500)/\sigma$, has only recently been demonstrated with certainty [2,3]. The difficulty comes from the especially short lifetime of the σ, which causes it to lack the simple narrow "bump" signature associated with longer-lived resonances. It is the use of dispersive analysis techniques [4], which build in constraints from the causality and crossing symmetry of scattering amplitudes, when applied to the experimental data, which have led to an unambiguous signal for a σ resonance. These techniques have ensured that the location of the corresponding pole singularity, located far into the complex energy plane, can now be stated with a high level of precision [5,6]. (We point readers to Refs. [7] for prior efforts to determine the σ pole using unitarized chiral perturbation theory.)

In principle, it should be possible within QCD to calculate the scalar, isoscalar $\pi\pi$ scattering amplitude and the contribution of the σ resonance to it, but the nonperturbative nature of the theory at low energies leaves us with limited calculational tools. The most powerful current approach is lattice QCD, in which the quark and gluon fields are discretized on a space-time grid of finite size, allowing numerical computation by averaging over large numbers of possible field configurations generated by Monte Carlo sampling. In particular, from the time dependence of correlation functions calculated in this way,

we can extract a discrete spectrum of states whose dependence on the volume of the lattice can be related to meson-meson scattering amplitudes [8,9].

Calculations of the scalar, isoscalar channel have long been considered to be among the most challenging applications of lattice QCD. In order to be successful here, it is necessary to evaluate all quark propagation diagrams contributing to the correlation functions, to reliably extract a large number of states in the spectrum, and to determine and interpret the energy dependence of the scattering amplitude in the elastic region. To date, no calculation has overcome all these challenges [10].

In this Letter, we show that by combining a number of novel techniques whose application we have pioneered over the past few years, we can meet all these challenges and provide the first determinations of the scalar, isoscalar scattering amplitude within QCD. By utilizing distillation [11], we are able to evaluate with good statistical precision all required quark propagation diagrams, including those which feature quark-antiquark annihilation. By diagonalizing matrices of correlation functions [12] using a large basis of composite QCD operators with relevant quantum numbers [13–19], we are able to make robust determinations of spectra, and by considering multiple lattice volumes and moving frames, we are able to map out the energy dependence of the $\pi\pi$ scattering amplitude over the entire elastic region. (We point the reader to Refs. [20] for parallel efforts in the study of elastic resonant amplitudes using similar techniques.)

We perform our calculations with two different values of the degenerate u, d quark mass, corresponding to pions with masses of approximately 236 and 391 MeV [21,22].

We find that for the lighter mass, the scattering amplitude is compatible with featuring a σ appearing as a broad resonance, which closely resembles the experimental situation. As the quark mass is increased, we find that the σ evolves into a stable bound state lying below the $\pi\pi$ threshold.

Correlation functions and the finite-volume spectrum.— The discrete spectrum of hadronic eigenstates of QCD in a finite volume is extracted from two-point correlation functions $C_{ab}(t, t'; \vec{P}) = \langle 0|\mathcal{O}_a(t, \vec{P})\mathcal{O}_b^\dagger(t', \vec{P})|0\rangle$, with spatial momentum $\vec{P} = (2\pi/L)[n_x, n_y, n_z]$, where $n_i \in \mathbb{Z}$ in an $L \times L \times L$ box. We use a large basis of interpolating fields $\mathcal{O}_a$ from two classes. The first are single-meson-like operators [13,14,17] which resemble a $q\bar{q}$ construction of definite momentum $(\bar{\psi}\Gamma\psi)_{\vec{P}}$, where Γ are operators acting in spin, color, and position space [11]. Both $u\bar{u} + d\bar{d}$ and $s\bar{s}$ flavor constructions are included [16,23]. The second class of operators are those resembling a pair of pions $\pi\pi$ with definite relative and total momentum $\sum_{\hat{p}_1, \hat{p}_2} w_{\vec{p}_1, \vec{p}_2; \vec{P}}(\bar{\psi}\Gamma_1\psi)_{\vec{p}_1}(\bar{\psi}\Gamma_2\psi)_{\vec{p}_2}$ [18], projected into isospin $= 0$. Each isovector pionlike operator is constructed as the particular linear superposition, in a large basis of single-meson operators, that maximally overlaps with the pseudoscalar ground state [17,18].

We compute matrices of correlation functions $C_{ab}(t, t'; \vec{P})$ using multiple single-meson operators along with several relative momentum constructions $\vec{p}_1 + \vec{p}_2 = \vec{P}$ of the $\pi\pi$-like operators. (We also include several $K\bar{K}$-like operators, of analogous construction to the $\pi\pi$ operators, although they are not vital in the determination of the spectrum below the $K\bar{K}$ threshold.) This kind of operator basis has been used successfully in the determination of scattering amplitudes in the $\pi\pi I = 1$ channel [19,22] and the coupled-channel $(\pi K, \eta K)$ [24] and $(\pi\eta, K\bar{K})$ [25] cases.

After integration over the quark fields appearing in the path-integral representation of $C_{ab}(t, t'; \vec{P})$, we find that a variety of topologies of quark propagation diagrams appear, shown schematically in Fig. 1. Correlators with $\pi\pi$-like operators at t and t', for instance, require both connected pieces $(a), (b)$ and partially (c) and completely (d)
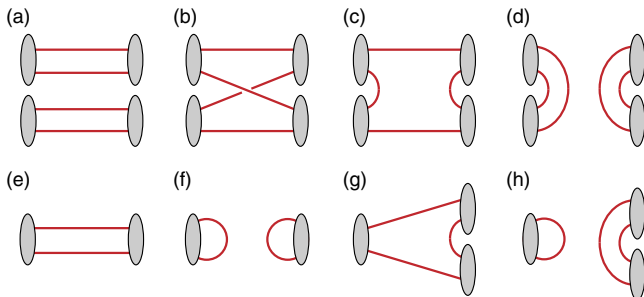
disconnected pieces which feature quark propagation from a time t to the same time t. Computation of these propagation objects has historically been a major challenge for lattice QCD. Within the distillation approach we utilize, determining these objects becomes manageable, and by obtaining them for all time slices t, good signals can be garnered by averaging correlation functions for fixed time separations over the whole temporal extent of the lattice. The factorization of operator construction, inherent in distillation, allows for the reuse of these propagation objects, and those used here have been previously computed and used in other projects that featured quark annihilation [19,22–27].

In Fig. 2, we show the contributions of the various diagrams to an example correlation function having an operator $\pi_{[000]}\pi_{[110]}$ at both $t' = 0$ and t, where we observe that all diagrams are evaluated with good statistical precision. In general, delicate cancellations between different contributing diagrams can be present in isoscalar correlation functions, and our approach is seen to be capable of accurately capturing these.

We computed correlation matrices for total momentum $\vec{P} = [000]$, [100], [110], [111], and [200], extracting multiple states in the spectrum of each using variational analysis of the type described in Ref. [14]. Details of the dynamical lattices, which include degenerate light u, d quarks and a heavier s quark, and which have spatial lattice spacing $a_s \sim 0.12$ fm, can be found in Refs. [21,22]. For the 391 MeV pion case, we computed with three lattice volumes, 16^3, 20^3, and 24^3, while for the 236 MeV pion
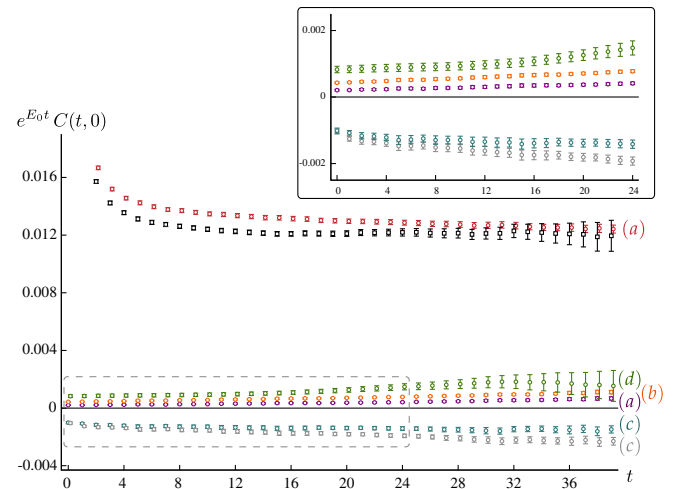

FIG. 2. Contributions of various diagrams [falling into the categories (a)–(d) presented in Fig. 1—two different variants each of (a) and (c) appear] to the correlation function having an operator $\pi_{[000]}\pi_{[110]}$ at both $t' = 0$ and t. The time dependence is weighted by $e^{E_0 t}$ with E_0 the energy of the lightest state with $\vec{P} = [110]$. The complete correlation function, which corresponds to the sum of the pieces shown, is shown by the black squares. Computation on a $32^3 \times 256$ lattice with $m_\pi = 236$ MeV.

FIG. 1. Schematic quark propagation diagrams which contribute to the isoscalar correlation functions required in this Letter.

case we used a single larger 32^3 volume. The extracted spectra are shown in Fig. 3. In this first study, we will restrict our attention to energies below the $K\bar{K}$ threshold from which we can determine the $\pi\pi$ elastic scattering phase shift.

Scattering amplitudes and the σ pole.—Under the well-justified approximation of neglecting kinematically suppressed higher partial waves, the $L \times L \times L$ finite-volume spectrum is related to the S-wave $\pi\pi$ elastic scattering phase shift by

$$\cot\delta_0(E_{\rm cm}) + \cot\phi(P,L) = 0, \qquad (1)$$

where $\phi(P,L)$ is a known function which differs according to $\vec{P}$ [8]. This provides a one-to-one mapping between the discrete finite-volume energies determined in lattice QCD and the infinite-volume scattering phase shift evaluated at those energies. (This equation is exact up to corrections due to the mixing with $\ell \geq 2$ amplitudes due to the reduction of
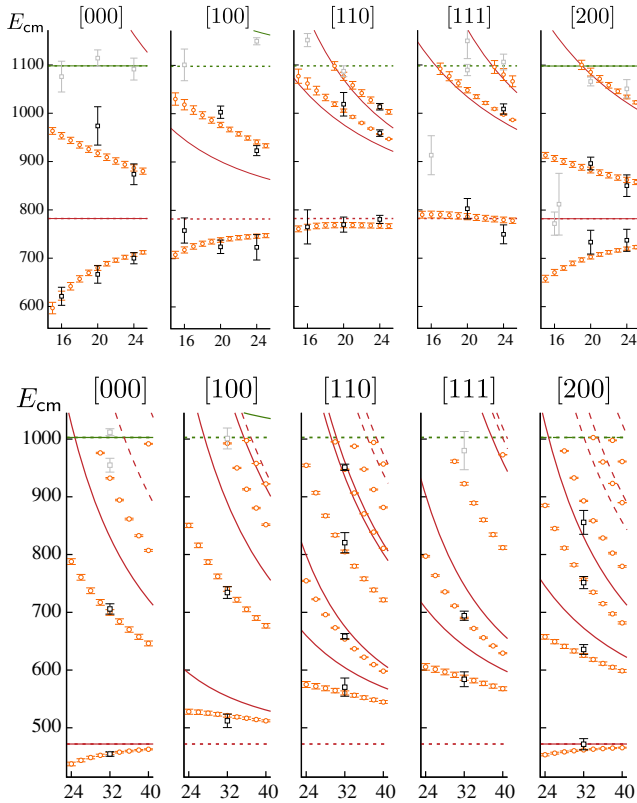
rotational symmetry [8]. We have addressed these effects for other systems in previous studies [18,19,22,24,25] and in this case find their contribution to be negligible.)

In Fig. 4, we present the phase shifts determined from the spectra shown in Fig. 3. A simple-minded approach to parametrizing the energy dependence of these scattering amplitudes neglects the explicit contribution of any left-hand cut—which is present due to crossing symmetry, but which is distant from the physical scattering region for heavy pions—leaving significant freedom in choice of functional form. We find that we can obtain good descriptions of the lattice spectra for many unitarity-preserving choices of parametrization—Fig. 4 shows one illustrative example, which uses a single-channel K matrix featuring a pole term plus a constant, and a Chew-Mandelstam phase space (see Ref. [24] and references therein), the corresponding description of the finite-volume spectrum being shown in orange in Fig. 3. In previous studies [19,22,24,25] of amplitudes featuring narrow resonances, we observed very little variation in the pole position of the resonance with parametrization choice variation.
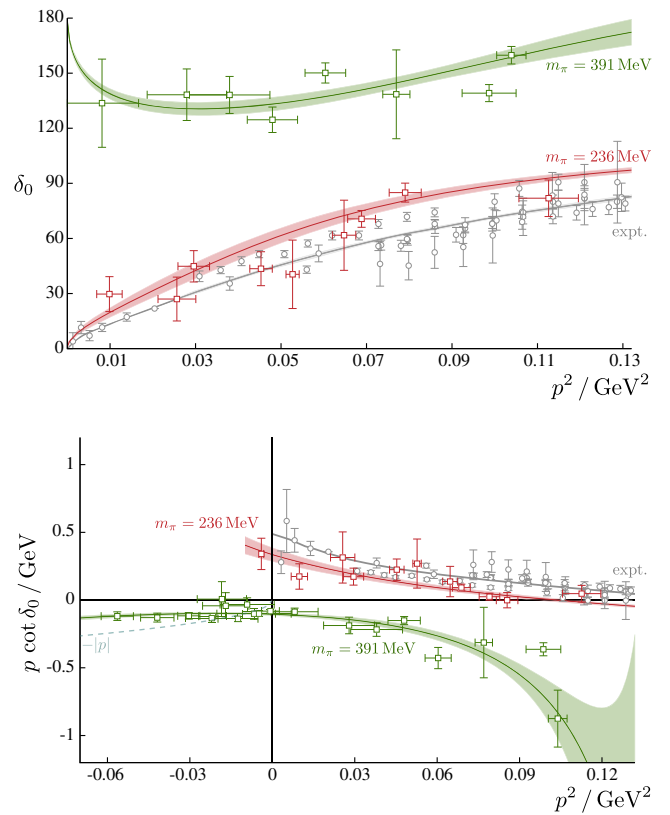

FIG. 3. Center-of-momentum frame energies (black and gray points) extracted from variational analysis of correlation matrices at five values of $\vec{P}$ plotted versus L. Upper panel shows spectra for $m_\pi = 391$ MeV and the lower panel for $m_\pi = 236$ MeV. The vacuum contribution to [000] correlation functions, which is time independent, and thermal contributions for other $\vec{P}$ are removed using the technique described in Ref. [18]. Red curves indicate noninteracting $\pi\pi$ energies. Small dashed red and green horizontal lines show the $\pi\pi$ and $K\bar{K}$ thresholds. Orange points show the finite-volume spectrum obtained from the K-matrix pole-plus-constant parametrization mentioned in the text.

FIG. 4. Upper panel: S-wave $\pi\pi$ elastic scattering phase shift δ_0 plotted against the scattering momentum $p^2 = (E_{\rm cm}/2)^2 - m_\pi^2$. Lower panel: Same data presented as $p\cot\delta_0$ (some points with large uncertainty have not been plotted). The colored curves are the result of a K-matrix pole-plus-constant with Chew-Mandelstam phase-space parametrization. The gray points show experimental data [1], and the gray curve shows the constrained dispersive description of these data presented in Ref. [3].

In the 391 MeV pion case, we find that all parametrizations which successfully describe the finite-volume spectra have a pole on the real energy axis below $\pi\pi$ threshold on the physical Riemann sheet, which we interpret as the σ appearing as a bound state of mass 758(4) MeV. Considering the amplitude determined with 236 MeV pions, we observe in Fig. 4 a qualitative change of behavior in the phase-shift curve to a form which does not resemble either that expected for a bound state or that of a narrow elastic resonance. We find that all successful descriptions of the spectrum have a pole on the second Riemann sheet with a large imaginary part, which we interpret as the σ appearing as a broad resonance. Because the amplitude, determined from the finite-volume spectrum, is only constrained on the real energy axis, which is far from the pole position, there is a significant variation in the precise determination of the location of the pole under reasonable variations of the parametrization form. Details of these forms can be found in Refs. [25] and in the Supplemental Material [28]. Given the important phenomenological role of the Adler zero, we consider some parametrizations that include it. The phenomenon of significant pole position variation has been previously observed when experimental $\pi\pi$ phase-shift data are used to fix parameters in amplitude models that do not build in dispersive constraints [5].

Figure 5 shows the complex energy plane illustrating the extracted pole position $s_0 = [E_\sigma - (i/2)\Gamma_\sigma]^2$ for a range of parametrization choices. We also show the coupling $|g_{\sigma\pi\pi}|$ extracted from the residue of the t matrix at the pole $g_{\sigma\pi\pi}^2 = \lim_{s \to s_0}(s_0 - s)t(s)$.

Summary and outlook.—In this Letter, we have, for the first time, determined the low-lying spectra of the scalar-isoscalar channel of QCD in a box, including all required quark propagation diagrams. From the finite-volume spectra, we have extracted the $\pi\pi$ elastic scattering amplitude which shows qualitatively different behavior at the two pion masses considered, 236 and 391 MeV, with the heavier mass featuring a σ appearing as a stable bound state.

The amplitude parametrizations we explored to describe the finite-volume spectrum determined with 236 MeV pions all feature a σ appearing as a broad resonance, but the pole position is not precisely determined, showing variation with parametrization choice. We believe that this comes about because our parametrizations, while maintaining elastic unitarity, do not necessarily respect the analytical constraints placed on them by causality and crossing symmetry. In the future, we plan to adapt dispersive approaches so that they are applicable to describing the lattice data, and we expect this will allow us to pin down the σ pole position with precision directly from QCD.

With constrained amplitude forms in hand, it will become appropriate to perform calculations with lighter u, d quarks, such that we move closer to the physical pion mass, in order to make direct comparison with the experimental situation. It will also be useful to examine
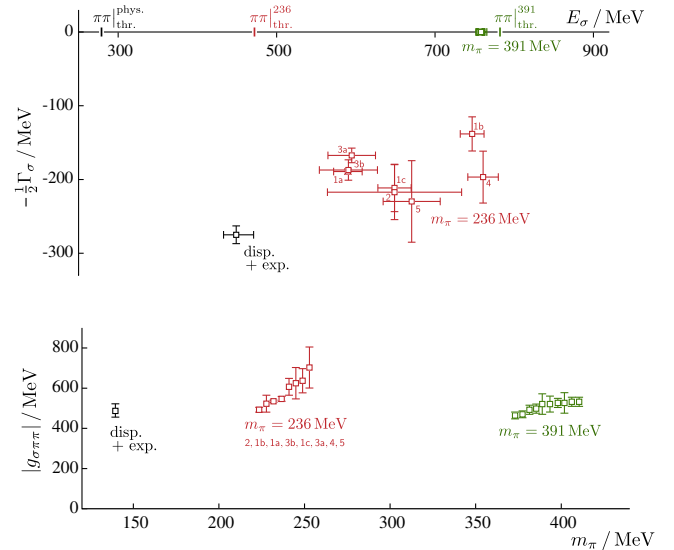

FIG. 5.   Upper panel: t-matrix pole positions for a variety of parametrizations: K-matrix pole-plus-polynomial forms (1a)–(1c) with and (2) without Chew-Mandelstam phase space and/or (3a),(3b) Adler zero [29], (4) relativistic Breit-Wigner, and (5) effective range expansion. See the Supplemental Material for a full description [28]. Green points: bound-state pole (physical sheet) at $m_\pi = 391$ MeV. Red points: resonant pole (unphysical sheet) at $m_\pi = 236$ MeV. Black point: Resonant pole from dispersive analysis of experimental data (conservative average presented in Ref. [5]). Lower panel: Coupling $g_{\sigma\pi\pi}$ from t-matrix residue at the pole—points from various parametrizations are shifted horizontally for clarity.

pion masses between the 236 and 391 MeV considered here to determine how the transition we have observed from bound state to resonance is manifested—a suggestion from unitarized chiral perturbation theory [30] has the coupling $g_{\sigma\pi\pi}$, which one might conclude from Fig. 5 is approximately independent of quark mass, having a divergent behavior somewhere near $m_\pi \sim 300$ MeV.

Our calculational techniques allow us to determine finite-volume spectra above the $K\bar{K}$ threshold, and by considering such energies within a coupled-channel analysis, we expect to be able to study any $f_0(980)$-like resonance that may appear. Such a state is anticipated as an isospin partner of the a_0 resonance which we observed near the $K\bar{K}$ threshold in a recent 391 MeV pion mass calculation [25]. A comprehensive study of the light scalar meson nonet (σ, κ, a_0, f_0) within first-principles QCD will then be possible. The finite-volume approach can also be extended to study the coupling of these states to external currents [26,27,31–36]—by examining the current virtuality dependence of the form factors evaluated at the resonance pole, we expect to be able to infer details of the constituent structure of the scalar mesons.

---

[*]briceno@jlab.org
[†]dudek@jlab.org
[‡]edwards@jlab.org
[§]d.j.wilson@damtp.cam.ac.uk

[1] S. D. Protopopescu, M. Alston-Garnjost, A. Barbaro-Galtieri, S. M. Flatte, J. H. Friedman, T. A. Lasinski, G. R. Lynch, M. S. Rabin, and F. T. Solmitz, Phys. Rev. D **7**, 1279 (1973); B. Hyams *et al.*, Nucl. Phys. **B64**, 134 (1973); G. Grayer *et al.*, Nucl. Phys. **B75**, 189 (1974); P. Estabrooks and A. D. Martin, Nucl. Phys. **B79**, 301 (1974).

[2] I. Caprini, G. Colangelo, and H. Leutwyler, Phys. Rev. Lett. **96**, 132001 (2006).

[3] R. Garcia-Martin, R. Kaminski, J. R. Pelaez, and J. Ruiz de Elvira, Phys. Rev. Lett. **107**, 072001 (2011).

[4] S. M. Roy, Phys. Lett. B **36B**, 353 (1971).

[5] J. R. Pelaez, Phys. Rep. **658**, 1 (2016).

[6] K. A. Olive *et al.* (Particle Data Group Collaboration), Chin. Phys. C **38**, 090001 (2014).

[7] A. Dobado and J. R. Pelaez, Phys. Rev. D **56**, 3057 (1997); J. A. Oller and E. Oset, Nucl. Phys. **A620**, 438 (1997); **A652**, 407(E) (1999); J. A. Oller, E. Oset, and J. R. Pelaez, Phys. Rev. Lett. **80**, 3452 (1998); Phys. Rev. D **59**, 074001 (1999); **75**, 099903 (2007).

[8] M. Luscher, Nucl. Phys. **B354**, 531 (1991); K. Rummukainen and S. A. Gottlieb, Nucl. Phys. **B450**, 397 (1995); P. F. Bedaque, Phys. Lett. B **593**, 82 (2004); C. h. Kim, C. T. Sachrajda, and S. R. Sharpe, Nucl. Phys. **B727**, 218 (2005); Z. Fu, Phys. Rev. D **85**, 014506 (2012); L. Leskovec and S. Prelovsek, Phys. Rev. D **85**, 114507 (2012); M. Gockeler, R. Horsley, M. Lage, U. G. Meissner, P. E. L. Rakow, A. Rusetsky, G. Schierholz, and J. M. Zanotti, Phys. Rev. D **86**, 094513 (2012).

[9] S. He, X. Feng, and C. Liu, J. High Energy Phys. 07 (2005) 011; M. Lage, U.-G. Meißner, and A. Rusetsky, Phys. Lett. B **681**, 439 (2009); V. Bernard, M. Lage, U. G. Meißner, and A. Rusetsky, J. High Energy Phys. 01 (2011) 019; M. Doring, U.-G. Meißner, E. Oset, and A. Rusetsky, Eur. Phys. J. A **47**, 139 (2011); M. Doring and U. G. Meißner, J. High Energy Phys. 01 (2012) 009; D. Agadjanov, U.-G. Meißner, and A. Rusetsky, J. High Energy Phys. 01 (2014) 103; M. Doring, U. G. Meißner, E. Oset, and A. Rusetsky, Eur. Phys. J. A **48**, 114 (2012); M. T. Hansen and S. R. Sharpe, Phys. Rev. D **86**, 016007 (2012); R. A. Briceno and Z. Davoudi, Phys. Rev. D **88**, 094507 (2013); P. Guo, J. J. Dudek, R. G. Edwards, and A. P. Szczepaniak, Phys. Rev. D **88**, 014501 (2013).

[10] M. G. Alford and R. L. Jaffe, Nucl. Phys. **B578**, 367 (2000); S. Prelovsek, T. Draper, C. B. Lang, M. Limmer, K.-F. Liu, N. Mathur, and D. Mohler, Phys. Rev. D **82**, 094507 (2010); Z. Fu, Phys. Rev. D **87**, 074501 (2013); M. Wakayama, T. Kunihiro, S. Muroya, A. Nakamura, C. Nonaka, M. Sekiguchi, and H. Wada, Phys. Rev. D **91**, 094508 (2015); D. Howarth and J. Giedt, arXiv:1508.05658; Z. Bai *et al.* (RBC and UKQCD Collaborations), Phys. Rev. Lett. **115**, 212001 (2015).

[11] M. Peardon, J. Bulava, J. Foley, C. Morningstar, J. Dudek, R. G. Edwards, B. Joo, H.-W. Lin, D. G. Richards, and K. J. Juge (Hadron Spectrum Collaboration), Phys. Rev. D **80**, 054506 (2009).

[12] C. Michael, Nucl. Phys. **B259**, 58 (1985); J. J. Dudek, R. G. Edwards, N. Mathur, and D. G. Richards, Phys. Rev. D **77**, 034501 (2008); B. Blossier, M. Della Morte, G. von Hippel, T. Mendes, and R. Sommer, J. High Energy Phys. 04 (2009) 094.

[13] J. J. Dudek, R. G. Edwards, M. J. Peardon, D. G. Richards, and C. E. Thomas, Phys. Rev. Lett. **103**, 262001 (2009).

[14] J. J. Dudek, R. G. Edwards, M. J. Peardon, D. G. Richards, and C. E. Thomas, Phys. Rev. D **82**, 034508 (2010).

[15] J. J. Dudek, R. G. Edwards, M. J. Peardon, D. G. Richards, and C. E. Thomas, Phys. Rev. D **83**, 071504 (2011).

[16] J. J. Dudek, R. G. Edwards, B. Joo, M. J. Peardon, D. G. Richards, and C. E. Thomas, Phys. Rev. D **83**, 111502 (2011).

[17] C. E. Thomas, R. G. Edwards, and J. J. Dudek, Phys. Rev. D **85**, 014507 (2012).

[18] J. J. Dudek, R. G. Edwards, and C. E. Thomas, Phys. Rev. D **86**, 034031 (2012).

[19] J. J. Dudek, R. G. Edwards, and C. E. Thomas (Hadron Spectrum Collaboration), Phys. Rev. D **87**, 034505 (2013); J. J. Dudek, R. G. Edwards, and C. E. Thomas (Hadron Spectrum Collaboration), Phys. Rev. D **90**, 099902 (2014).

[20] J. Bulava, B. Fahy, B. Horz, K. J. Juge, C. Morningstar, and C. H. Wong, Nucl. Phys. **B910**, 842 (2016); G. S. Bali, S. Collins, A. Cox, G. Donald, M. Gockeler, C. B. Lang, and A. Schafer (RQCD Collaboration), Phys. Rev. D **93**, 054509 (2016); S. Aoki *et al.* (CS Collaboration), Phys. Rev. D **84**, 094505 (2011); X. Feng, K. Jansen, and D. B. Renner, Phys. Rev. D **83**, 094505 (2011); S. Aoki *et al.* (CP-PACS Collaboration), Phys. Rev. D **76**, 094506 (2007).

[21] H.-W. Lin *et al.* (Hadron Spectrum Collaboration), Phys. Rev. D **79**, 034502 (2009).

[22] D. J. Wilson, R. A. Briceno, J. J. Dudek, R. G. Edwards, and C. E. Thomas, Phys. Rev. D **92**, 094502 (2015).

[23] J. J. Dudek, R. G. Edwards, P. Guo, and C. E. Thomas (Hadron Spectrum Collaboration), Phys. Rev. D **88**, 094505 (2013).

[24] J. J. Dudek, R. G. Edwards, C. E. Thomas, and D. J. Wilson (Hadron Spectrum Collaboration), Phys. Rev. Lett. **113**, 182001 (2014); D. J. Wilson, J. J. Dudek, R. G. Edwards, and C. E. Thomas, Phys. Rev. D **91**, 054008 (2015).

[25] J. J. Dudek, R. G. Edwards, and D. J. Wilson (Hadron Spectrum Collaboration), Phys. Rev. D **93**, 094506 (2016).

[26] R. A. Briceno, J. J. Dudek, R. G. Edwards, C. J. Shultz, C. E. Thomas, and D. J. Wilson, Phys. Rev. Lett. **115**, 242001 (2015).

[27] R. A. Briceño, J. J. Dudek, R. G. Edwards, C. J. Shultz, C. E. Thomas, and D. J. Wilson, Phys. Rev. D **93**, 114508 (2016).

[28] See Supplemental Material at http://link.aps.org/supplemental/10.1103/PhysRevLett.118.022002 for details of amplitude parameterizations.

[29] S. L. Adler, Phys. Rev. **137**, B1022 (1965).

[30] C. Hanhart, J. R. Pelaez, and G. Rios, Phys. Rev. Lett. **100**, 152001 (2008); J. Nebreda and J. R. Pelaez, Phys. Rev. D **81**, 054035 (2010).

[31] R. A. Briceño, M. T. Hansen, and A. Walker-Loud, Phys. Rev. D **91**, 034501 (2015).

[32] R. A. Briceño and M. T. Hansen, Phys. Rev. D **92**, 074509 (2015).

[33] R. A. Briceño and M. T. Hansen, Phys. Rev. D **94**, 013008 (2016).

[34] V. Bernard, D. Hoja, U. G. Meißner, and A. Rusetsky, J. High Energy Phys. 09 (2012) 023.

[35] A. Agadjanov, V. Bernard, U. G. Meißner, and A. Rusetsky, Nucl. Phys. **B886**, 1199 (2014).

[36] L. Lellouch and M. Luscher, Commun. Math. Phys. **219**, 31 (2001).

[37] R. G. Edwards and B. Joo, (SciDAC, LHPC, and UKQCD Collaborations), Nucl. Phys. B, Proc. Suppl. **140**, 832 (2005).

[38] M. A. Clark, R. Babich, K. Barros, R. C. Brower, and C. Rebbi, Comput. Phys. Commun. **181**, 1517 (2010).

[39] R. Babich, M. A. Clark, and B. Joo, in *Proceedings of the ACM/IEEE International Conference of High Performance Computing, Networking, Storage and Analysis, SC 10 (Supercomputing 2010), New Orleans, Louisiana, 2010.*

[40] K. Clark, B. Joo, A. Strelchenko, M. Cheng, A. Gambhir, and R. Brower, in *Proceedings of the ACM/IEEE International Conference of High Performance Computing, Networking, Storage and Analysis, SC 16, Salt Lake City, Utah, 2016.*

[41] B. Joó, D. Kalamkar, K. Vaidyanathan, M. Smelyanskiy, K. Pamnany, V. Lee, P. Dubey, and W. Watson, in *Supercomputing*, Lecture Notes in Computer Science, Vol. 7905, edited by J. Kunkel, T. Ludwig, and H. Meuer (Springer, Berlin, 2013), p. 40.

[42] J. C. Osborn, R. Babich, J. Brannick, R. C. Brower, M. A. Clark, S. D. Cohen, and C. Rebbi, *Proc. Sci.*, LATTICE2010 (2010) 037, arXiv:1011.2775.

[43] R. Babich, J. Brannick, R. C. Brower, M. A. Clark, T. A. Manteuffel, S. F. McCormick, J. C. Osborn, and C. Rebbi, Phys. Rev. Lett. **105**, 201602 (2010).